J Mater Sci (2008) 43:6890–6901
DOI 10.1007/s10853-008-2997-z

Magneto-microstructural coupling during stress-induced phase transformation in $Co_{49}Ni_{21}Ga_{30}$ ferromagnetic shape memory alloy single crystals

D. Niklasch · J. Dadda · H. J. Maier · I. Karaman

Received: 26 February 2008 / Accepted: 8 September 2008 / Published online: 27 September 2008

Abstract The present study reports on direct magneto-microstructural observations made during the stress-induced martensitic transformation in $Co_{49}Ni_{21}Ga_{30}$ alloy single crystals with optical, scanning electron, and magnetic force microscopy (MFM). The evolution of the microstructure and the associated magnetic domain morphology as a function of applied strain were investigated in the as-grown condition and after thermo-mechanical training. The results demonstrated that the stress-induced martensite (SIM) evolves quite differently in the two conditions and depending on the martensite formation mechanisms, the magnetic domain configuration was dissimilar. In the as-grown crystals two twin-related martensite variants were formed and the growth of these twin variants resulted in large strain. After thermo-mechanical training a morphology similar to a self-accommodating martensite structure was present at the initial stages of the transformation and thereafter martensite reorientation (MR) was the main transformation mechanism. The magnetic domains were found to be superimposed on the nano-scaled martensite twins in the as-grown condition, whereas training brought about the formation of domains on the order of a few microns without showing the one-to-one correspondence between domains and the twin structure. After the thermo-mechanical training detwinning at high-strain levels led to the formation of stripe-like domain structures. The ramifications of the results with respect to the magneto-microstructural coupling that may cause the magnetic shape memory effect (MSME) in Co–Ni–Ga alloys under constant external stress is addressed.

D. Niklasch (✉) · J. Dadda · H. J. Maier
Lehrstuhl für Werkstoffkunde (Materials Science), University of Paderborn, Pohlweg 47-49, 33098 Paderborn, Germany
e-mail: dorothee.niklasch@uni-paderborn.de

I. Karaman
Department of Mechanical Engineering, Texas A&M University, College Station, TX 77843, USA

Introduction

Ferromagnetic shape memory alloys (FSMAs) have attracted increasing interest in recent years because of their ability to show high reversible magnetic field-induced strain (MFIS) [1–5]. In contrast to the thermoelastic shape memory effect, the magnetic shape memory effect (MSME) can proceed with a higher rate and can be more efficient in terms of power throughput than the conventional shape memory effect. The fast reaction times in combination with the high MFIS (on the order of 5–10%) make the FSMAs promising materials for sensor and actuator applications.

The MSME can be triggered by two different mechanisms. First, the application of a magnetic field can lead to a reorientation of martensite twins by twin-boundary motion, in analogy to the stress-induced deformation in a conventional twinned martensitic shape memory alloy. Second, it can result from a magnetic field-induced phase transformation. However, the required magnitude of the magnetic field for the latter is often too large for actual FSMA applications [6].

The MSME resulting from twin-boundary motion in the martensitic phase was first reported by Ullakko et al. [1], and based on their findings several models were proposed [7–9]. The essential requirements for the incidence of the MSME are high magnetocrystalline anisotropy energy (MAE) and low energy for twin-boundary motion. If the MAE of a material is sufficiently large, an application of a magnetic

field can cause twin-boundary motion to increase the volume fraction of the twin variant with the energetically favored magnetization direction. In this manner, the twin variants having the easy magnetization axis along the applied field grow at the expense of the less favorably oriented ones instead of magnetization rotation. Therefore, the knowledge of the relation between the regions of uniform magnetization, i.e., the magnetic domains, and the twinned martensitic microstructure is essential for optimizing the MSME.

This relation has been studied by several techniques for different FSMAs. Magnetic force microscopy (MFM) [10], scanning electron microscopy (SEM) [11], interference-contrast-colloid technique (ICC) [12], Lorentz microscopy, and electron holography [13–15] have been used to examine the interaction of magnetic domains and the martensite twin structure in Ni–Mn–Ga, Co–Ni–Al, Ni–Fe–Ga, and Fe–Pd alloys. All studies confirmed the magneto-elastic coupling between the magnetic domains and martensite, but they are restricted only to thermally induced martensite. Thus, there currently is no information regarding the correlation between stress-induced martensite (SIM) and magnetic domain structure in the literature. Stress can assist the MSME and reduce the required field magnitudes to trigger field-induced shape change. For instance, high actuation stress levels and low magnetic field magnitudes were reported for Ni–Mn–Ga alloys showing a stress-assisted magnetic field-induced phase transformation [16–18]. However, before actual actuators can be designed that are based on this mechanism, it is important to identify the correlation between the magnetic domains and the microstructure and to understand the kinetics of phase and twin-boundary motion during the stress-assisted MSME.

Therefore, the present study was undertaken to examine the magneto-elastical coupling under external stress. The material investigated is a recently discovered Co–Ni–Ga alloy, which is known to exhibit promising shape memory characteristics in the vicinity of the Heusler composition [19, 20]. The structural, magnetic, and thermo-mechanical properties of Co–Ni–Ga alloys have been discussed elsewhere [21–24]. However, data on the interaction of magnetic domains and martensite twin structure in Co–Ni–Ga alloys are very limited, and the few studies that have been carried out on these alloys with regard to magneto-elastical-coupling addressed only thermally induced martensite [25–28]. Chernenko et al. [21] assumed that a large MFIS is hardly possible in Co–Ni–Ga single crystals in the martensitic state due to the low magnetic anisotropy energy and the high stress for MR as compared to a Ni–Mn–Ga alloy. However, as demonstrated in the present study, Co–Ni–Ga alloys provide the opportunity to show a MFIS under constant external stress. After exceeding the critical stress for the forward transformation, only small changes in stress are needed to increase the strain through phase boundary motion and MR. In addition, training effects can reduce the external stress required for twin-boundary motion.

Experimental

The alloy investigated was cast to a nominal composition of Co–21Ni–30 Ga (at.%) using vacuum induction melting. Single crystals were grown in a He atmosphere utilizing the Bridgman technique. Samples with dimensions of 4 mm × 4 mm × 8 mm were electro-discharge machined from the bulk single crystals such that the compression axes were along the [001] orientation. The austenite finish (A_f) temperature of the present alloy system was determined as 14 °C [22], so that the single crystals used in this study exhibited pseudoelasticity (PE) at room-temperature.

The PE experiments were conducted using an MTS servo-hydraulic test frame. Strain measurements were accomplished with the aid of a 3 mm-gage length miniature MTS extensometer mounted directly onto the sample. In order to monitor the morphology of the SIM and the magnetic domains at different strain levels, in-situ experiments were carried out using a custom-built mobile miniature load frame that allowed for studying the samples under load using optical microscopy (OM), electron backscatter diffraction (EBSD), and MFM. Prior to these experiments, one of the $[210]_a$-side-surfaces of the crystals was mechanically and then electro polished in order to remove any preparation-induced artifacts in the surface layer, which is known to be a key pre-condition for studies of magnetic domain structures [29].

A SEM equipped with an EBSD-system was operated at a nominal voltage of 20 kV to obtain orientation maps. The EBSD measurements were realized with an orientation imaging microscopy (OIM) system provided by TexSEM-Laboratories (TSL). The crystal structures and the corresponding lattice parameters of the austenite and martensite phases in Co–Ni–Ga alloys determined by Oikawa et al. [30] were used for indexing the phases detected by the EBSD-system. The austenite has B2 structure with a = 2.86 Å and the martensite crystal structure is $L1_0$ with a = 3.91 Å and c = 3.15 Å. In addition, energy dispersive X-ray spectroscopy (EDS) system equipped in SEM was used for the local phase analysis.

For imaging the magnetic domains in exactly the same areas as examined by OM and EBSD, a Digital Instruments Dimension 3100 MFM was used. The topography was first obtained in tapping mode and then the magnetic contrast was measured at a constant height of 100 nm in lift mode. Standard MFM CoCr tips were used as stray field sensors with the tip magnetization perpendicular to the sample surface.

After examining the as-grown crystals, iso-stress thermal cycles were employed as a training method. The samples were thermally cycled ten times at 25 MPa between temperatures of −120 °C and 140 °C and then another ten cycles at 50 MPa were conducted in the same temperature range. Heating/cooling of the sample was achieved by direct flow of hot/cold nitrogen gas onto the sample. After the initial PE experiments, the trained samples were also examined at the same strain levels (1% and 3% strain) using OM, EBSD, and MFM to compare the microstructure and magnetic domain morphology with those of the as-grown samples.

Results

Stress-induced martensite in the as-grown and thermo-mechanically trained crystal

Figure 1a and b shows the PE response of a [001]-oriented Co–Ni–Ga single crystal in its as-grown and trained state at room-temperature with a maximum strain of 4.2%, respectively. It is apparent from the figures that the training led to a decrease in critical stress for the forward transformation (σ_{crit}^{for}) and plateau stress ($\sigma_{plateau}$) from 70 MPa in the as-grown condition to 48 and 65 MPa, respectively. Note that the value of $\sigma_{plateau}$ is the same as that of σ_{crit}^{for} for the crystal in the as-grown state as seen in Fig. 1a. The drop in critical stress levels is attributed to the favorable internal stresses that were developed during the training that aid the forward transformation. Moreover, the unaltered values of the critical stress for the reverse transformation ($\sigma_{crit}^{rev} = 40$ MPa), and the stress hysteresis ($\Delta\sigma = 30$ MPa), for both cases indicate a very small influence of deformation history on the onset of the reverse transformation and the dissipated energy (stress hysteresis) in the present alloy system at room-temperature.

It is also clear from Fig. 1b that the SIM transformation proceeds in a more gradual manner after the proposed training reflecting a dissimilar microstructural evolution in the martensite phase. In order to gain further insight into this behavior, systematic in-situ observations were made using OM, EBSD, and AFM at different stages along the loading-plateau region of the stress–strain curves marked as **A** and **B** in Fig. 1, which correspond to 1 and 3% strain, respectively.

Electron backscatter diffraction was employed to detect the presence of the martensite variants and roughly estimate their respective volume fractions in the various areas of the sample. Previous transmission electron microscopy studies conducted on a companion Co–Ni–Ga single crystal [24] have revealed that the twin size in the present material is about 40 nm and that one twin variant has a greater

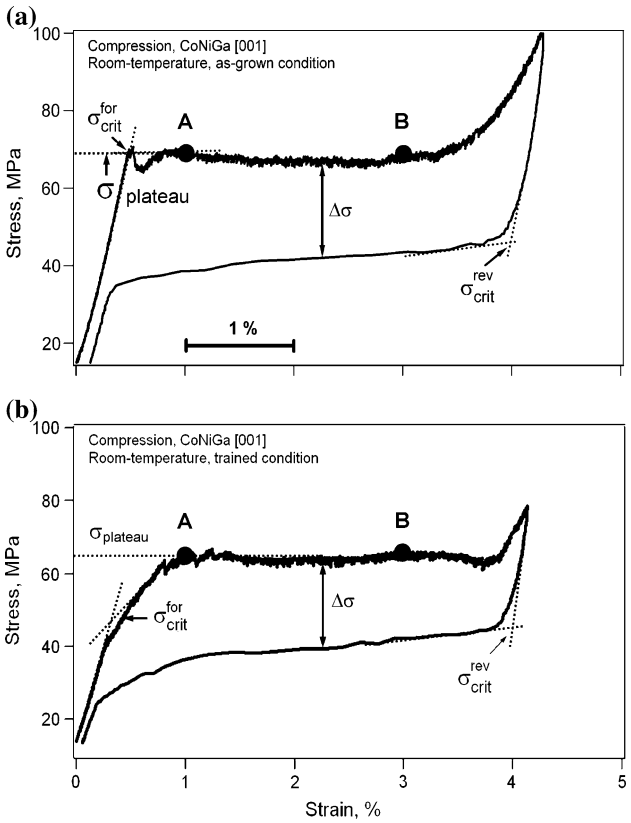

Fig. 1 Stress–strain response of the Co–Ni–Ga [001]-oriented single crystal (**a**) in the as-grown and (**b**) in the thermo-mechanically trained conditions at room-temperature showing near perfect pseudoelastic behavior. The plateau stress ($\sigma_{plateau}$), the critical stresses for the forward (σ_{crit}^{for}) and the reverse transformations (σ_{crit}^{for}) and the stress hysteresis ($\Delta\sigma$) are also defined. The points A and B on the curves indicate the applied strain levels in the experiments conducted to study the microstructure and magnetic domain structure present under applied load

volume fraction. Thus, the electron beam of the EBSD-system, which has an effective size of about 200 nm, will always probe many twin-related martensite variants as depicted schematically in Fig. 2a.

As a result, the experimentally obtained EBSDs consisted of a strong Kikuchi pattern superimposed by a weaker one resulting from the variant with the lower volume fraction, cf. Figure 2b. When operated in automatic mode, the EBSD-system can only index the variant with the larger volume fraction (Fig. 2c), and manual identification of Kikuchi bands (Fig. 2d) was needed to obtain the orientation of the second variant. In the remainder of this paper, brackets will be used to designate the variant with the lower volume fraction.

Figure 3a displays the microstructure of the as-grown crystal at 1% strain demonstrating a lamellar martensitic morphology (**M**) coexisting with the untransformed matrix, i.e., austenite marked as **A** in the figure. The martensite plates consist of twin-related variants labeled as V_1 and V_2.

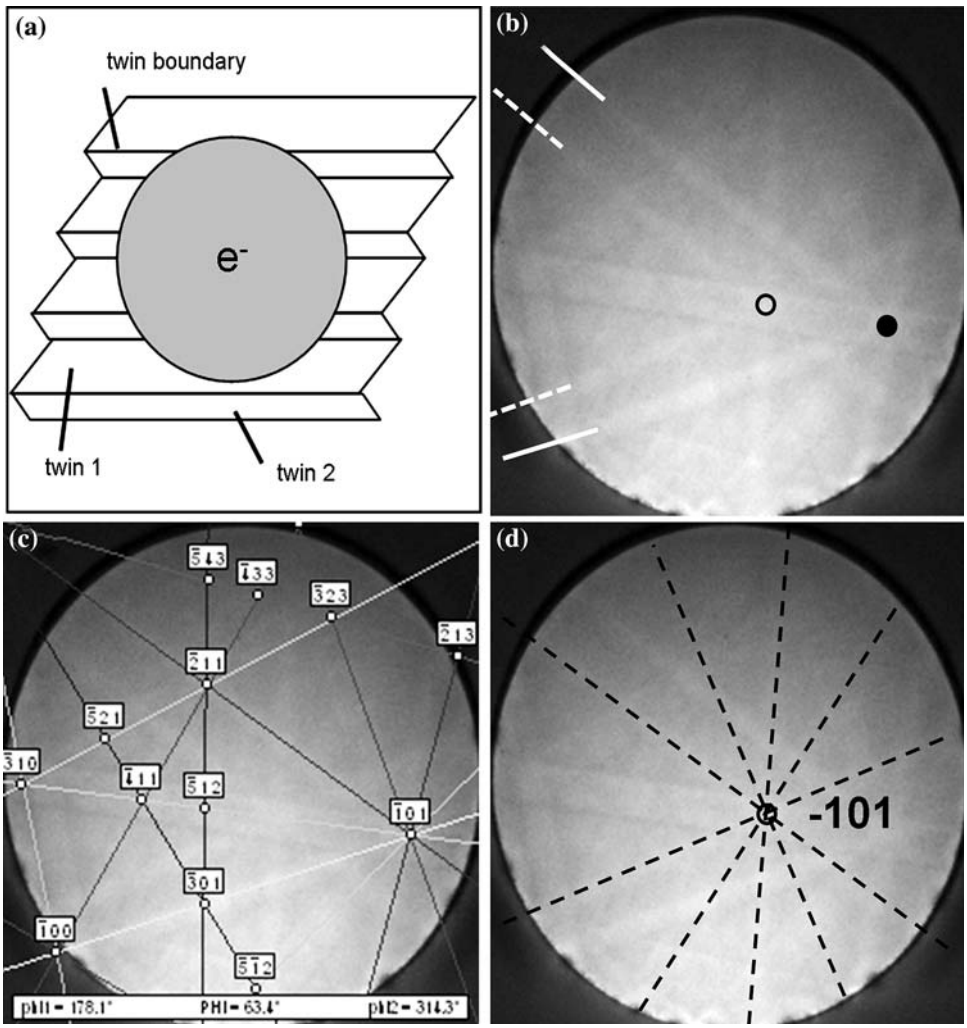

Fig. 2 **a** Schematic showing the microstructure probed by the EBSD-system, **b** actual superimposed diffraction pattern with the weak second component marked by dashed lines; open and full circle represent corresponding zone axes from the variants with low and high volume fraction, **c** indexed diffraction pattern revealing the dominant twin variant and **d** the weaker Kikuchi pattern from twin 2 being identified with dashed lines

The latter has low volume fraction, and thus, is set in brackets in Fig. 3a. The martensite plates that have a direct interface with the austenite are known as habit plane variants, while the twin-related variants such as V_1 and V_2 are called correspondence variant pairs (CVPs) and are separated by a twin boundary. The orientations of V_1 and V_2 were determined to be identical with reference to the loading axis, i.e., $[110]_M$ is parallel to $[001]_A$ as shown in Fig. 3b. The difference in the variants can easily be realized from the inverse pole figure produced with respect to one of the surface normals ($[210]_A$) as shown in Fig. 3c, i.e., the variants V_1 and V_2 have their crystallographic directions $[221]_M$ and $[112]_M$ perpendicular to the loading axis of the sample. A further increase in strain to 3% (point B in Fig. 1a) results in the growth of the martensite plates as shown in Fig. 3d. The transformation is almost complete at this strain level. Note that the variant V_2 has the higher volume fraction in regions with residual austenite.

The changes in microstructural evolution caused by the thermo-mechanical training are shown in Figs. 4 and 5 at 1 and 3% strain, respectively. Figure 4a–c represents the microstructures taken from different locations of the sample deformed to 1% strain. It is clear from the figure that the thermo-mechanical training leads to the formation of multiple internally twinned martensite plates forming a self-accommodating morphology, and as shown in Fig. 4a–c, the microstructure after training also became more heterogeneous. This change in microstructure is also reflected by the difference in the critical transformation strain levels in as-grown and trained samples (Fig. 1). Some areas still showed the variants V_1 and V_2, which were already present in the as-grown crystal. In addition, new CVPs namely V_3 and V_4 were observed (Fig. 4b and c). These two variants have their $[102]_M$ and $[101]_M$ orientations parallel to the loading axis of the sample (Fig. 4d). Again, weak superimposed EBSD patterns were recorded in the areas where the additional variants V_3 and V_4 had formed. This indicates the presence of twin-related variants for V_3 and V_4 as well and these are designated as V_x and V_y. However, due to their very low volume fraction the Kikuchi bands of these

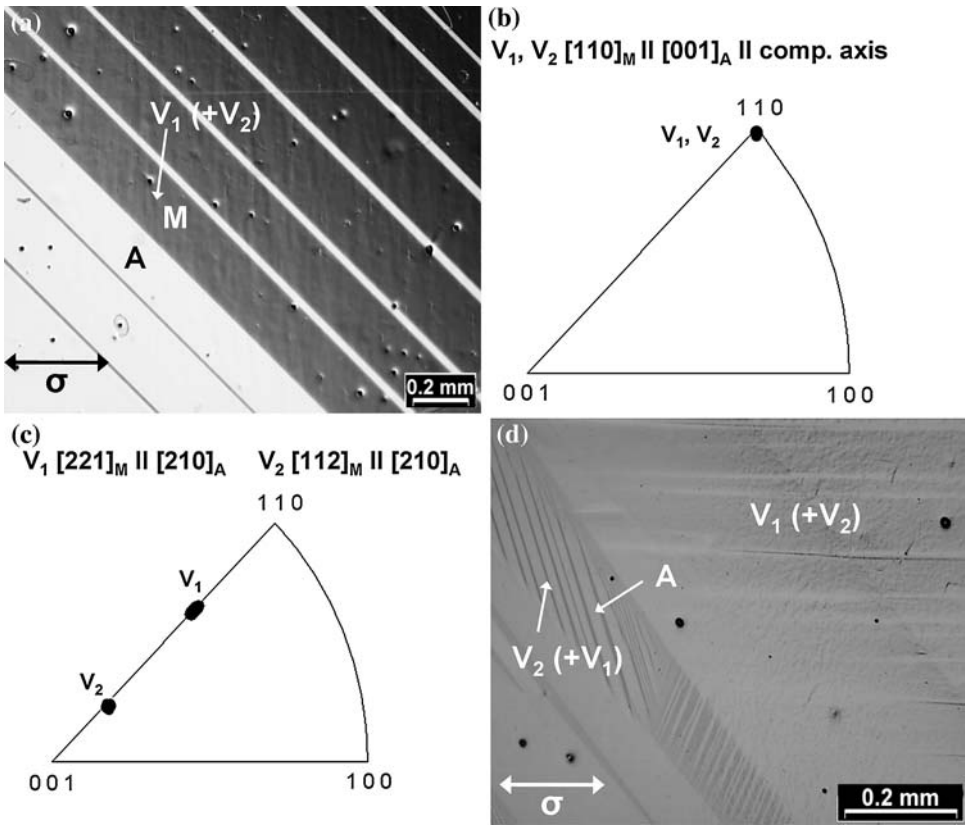

Fig. 3 **a** Formation of the stress-induced twin variants V_1 and V_2 from the austenite phase, A, at 1% strain in the as-grown crystal; the inverse pole figures parallel **b** and normal **c** to the compression axis. **d** Optical micrograph showing the microstructure at 3% strain in the as-grown crystal. See main text for details

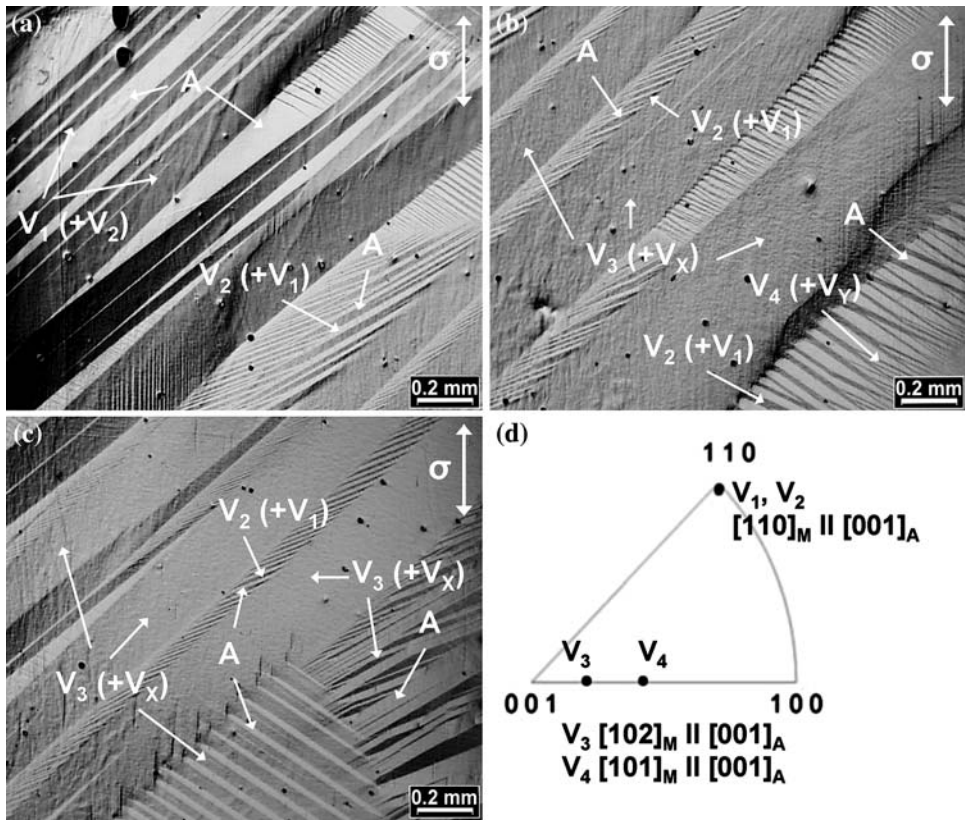

Fig. 4 **a–c** Optical micrographs of the thermo-mechanically trained crystal recorded after straining to 1% showing a self-accommodating martensite morphology **d** Inverse pole figure illustrating the orientations of the twin variants V_1, V_2, V_3, and V_4 with respect to the compression axis

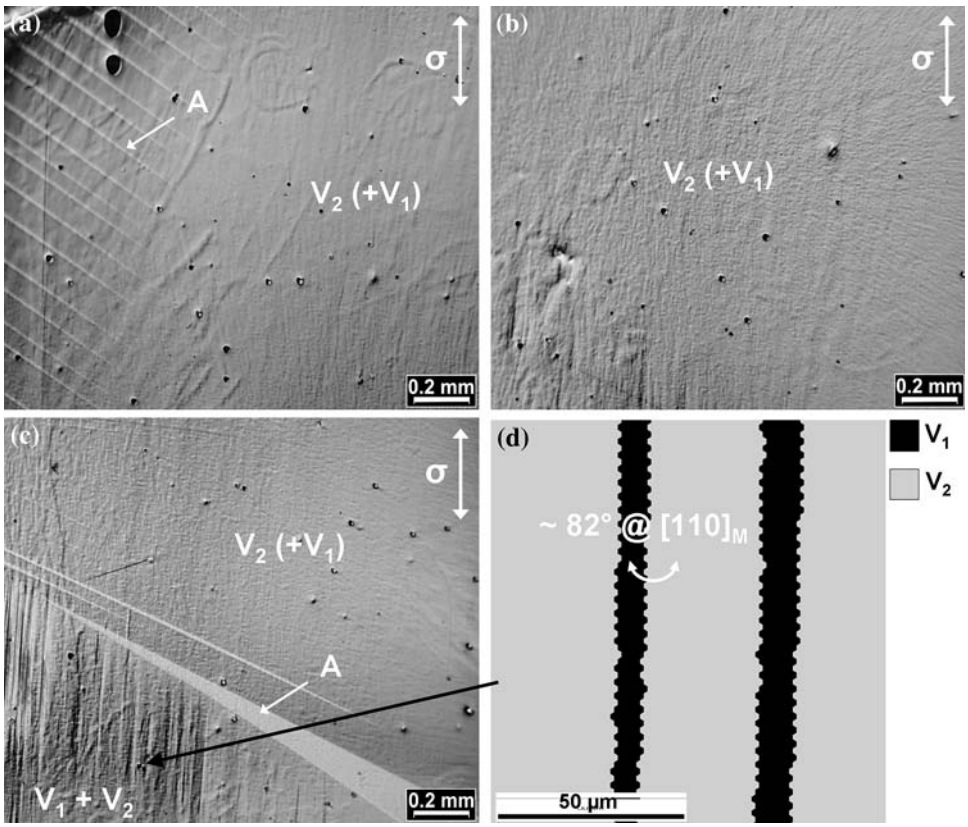

Fig. 5 **a–c** Optical micrographs presenting the microstructure upon straining to 3% for the same area as in Fig. 4a–c. **d** EBSD-map recorded within the detwinned area in the lower left part of (**c**) (indicated by an arrow) showing the orientation relationship between the twin variants V_1 and V_2

twin variants were too weak to be indexed manually, and thus are not included in Fig. 4d.

Figure 5a–c represents micrographs that were recorded when the sample was deformed to 3% strain, i.e., point B on the stress–strain curve shown in Fig. 1b. These microstructures were captured from the same locations as in Fig. 4a–c and the pores present on the surface of the sample can be used as reference points. It is clear from the Fig. 5a–c that the loading to 3% strain resulted in the growth of the twin variants V_1 and V_2 at the expense of the other variants observed at 1% loading strain, cf. Fig. 4a–c. It should be noted that variant V_2 is favored after thermo-mechanical training instead of the twin variant V_1, which is dominant in the as-grown crystal (Fig. 2a–c). This change in microstructure is also reflected by the difference in the plateau stress in as-grown and trained samples (Fig. 1).

Figure 5d displays the orientation map of the twin-related variants V_1 and V_2 taken from the bottom left corner region of the microstructure as pointed out in Fig. 5c. The coarsening of these twin variants is linked to the completeness of the transformation and to a partial detwinning process in this area as the applied strain (3%) is near the end of the plateau regime. Although the size of both twin variants V_1 and V_2 increased, V_2 still remains dominant and would probably grow by consuming V_1 upon further loading. From Fig. 5d, the misorientation angle between these variants is determined to be 82° around the $[110]_M$ axis and may be used to evaluate the orientation relationship between V_1 and V_2. The same misorientation angle between neighboring twins has been reported for Ni–Mn–Ga alloys [31].

Magnetic domain structure in the as-grown and thermo-mechanically trained crystal

Figure 6a shows a MFM image of the stress-free austenite phase demonstrating a single magnetic domain morphology, which is a commonly observed feature in several FSMAs such as Ni–Mn–Ga and Fe–Pd. [12, 28, 32, 33]. In addition, the apparent protrusions with a significant magnetic contrast in Fig. 6a are due to the presence of Co-rich γ-precipitates in the present Co–Ni–Ga alloy system.

Figure 6b displays the magnetic domain morphology of the as-grown crystal loaded to 1% strain and the scanned area corresponds to a subframe in Fig. 2a. The magnetic contrast results from small micro-domains (<0.5 µm), which are almost parallel to the compression axis. Note that these domain-lines also extend into the regions of untransformed austenite and the aforementioned single-domain morphology does no longer exist in the austenite.

The small micro-domains are still present in the crystal with twin variants V_1 and V_2 and in the residual austenite even at 3% strain as shown in Fig. 6c and d. In Fig. 6d, the two-phase region of residual austenite and martensite with

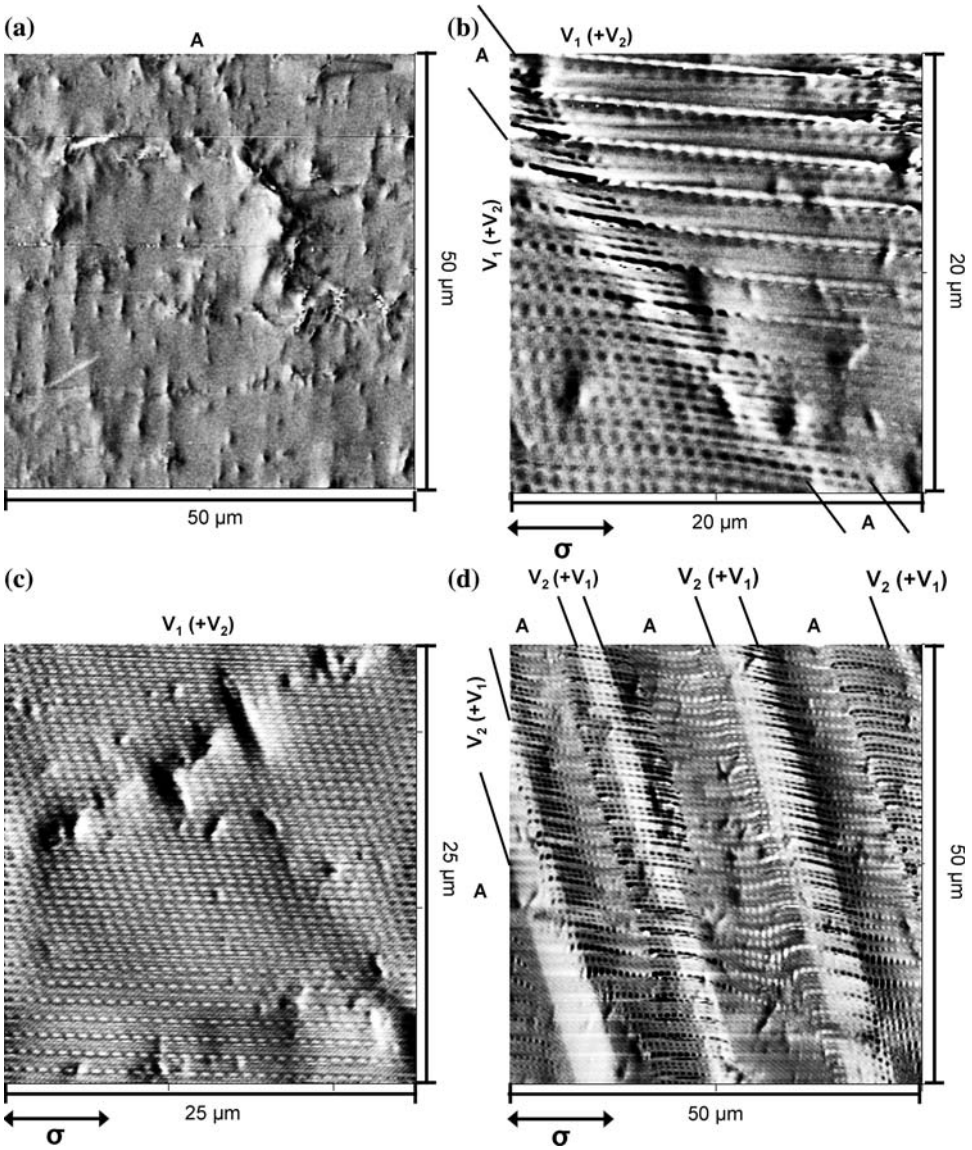

Fig. 6 MFM images of the as-grown crystal showing **a** the stress-free austenite phase, **b** a two-phase region of austenite (marked with A) and twin variants V_1 and V_2 at 1% strain, **c** a fully transformed area at 3% strain and **d** needle-shaped martensite within untransformed austenite at 3% strain. Note that the areas shown in **b–d** are small subframes of those seen in Fig. 2a (lower left part) and b (middle and upper left part), respectively

the dominant variant V_2 demonstrates a variation in the overall magnetization direction. The brighter appearing martensite plates indicate a more attractive out-of-plane magnetization in the martensite than in the austenite regions.

It should also be noted that the contrast from the micro-domains is not uniform as seen in Fig. 6b–d. This inhomogeneity is attributed to the Moiré-effect that can be arise in atomic force microscopy when there is a mismatch between the size of the magnetic domain structure and the scanning line grating [34, 35]. Therefore, the resolution of the scan was successively increased until the actual domain structures were captured. Figure 7a shows these domain structures in a completely transformed region of martensite with higher volume fraction of the twin variant V_1. The domain structures are on the order of the twin size observed by TEM elsewhere [24]. The fact that one twin (V_1) is wider than the other (V_2) is also visible in the magnetic domain structure. Figure 7b shows a schematic illustrating the correlation between the domain and twin structure. It can easily be perceived from Fig. 7 that there is a one-to-one correspondence between the magnetic domain and the twin structure in the as-grown crystal. In addition, it can also be seen from Fig. 7a that each twin is divided into magnetic domains with alternating magnetization directions. However, the details of the fine internal structures of the magnetic domains could not be resolved owing to their minute sizes in the present alloys.

Figure 8a and b shows MFM images of a trained crystal at 1% strain (point **A** in Fig. 1b). The domains in this case are on the order of several micrometers, which is significantly larger than that observed in the as-grown crystal seen in Fig. 6. This suggests that the changes in microstructure induced by the thermo-mechanical training

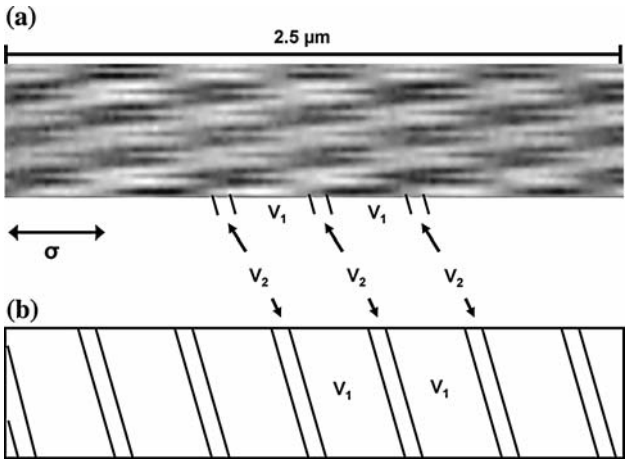

Fig. 7 **a** Actual magnetic domain structure as obtained by a high-resolution MFM scan within the martensite matrix and **b** corresponding schematic illustrating the one-to-one correspondence between twin variant V_1 and twin variant V_2 and the magnetic domain structure

also affected the magnetic domain configuration. Figure 8a displays supplementary domains at the interfaces between austenite and martensite needles with a higher volume fraction of the twin variant V_3. The supplementary domains form a fir tree type pattern, in which the magnetic flux is distributed by 90° domains as indicated by the arrows. By contrast, in areas, in which austenite and martensite needles with a higher volume fraction of the twin variant V_2 coexist, 180° domain structures are present (Fig. 8b). In this case the transitions (domain walls) show up as fine black or white lines, which can be attributed to 180° domain structures as marked by the arrows. This kind of domain pattern was found at mostly all interfaces between austenite and martensite shown in Fig. 4a–c. The fir tree pattern was only present at the lower middle part in Fig. 4c.

In Fig. 8c, the growth of the twin variants V_1 and V_2 after the increase in strain to 3% leads to the formation of a single-domain structure in the trained crystal similar to that observed in the stress-free austenite phase. However, the MFM image in Fig. 8d demonstrates stripe-like 180° domain structures in the region where the partial detwinnig took place (cf. Fig. 5d). Note that these domains are 10-fold greater in size as compared to the domains observed in the as-grown crystal (Figs. 6b–c and 7a).

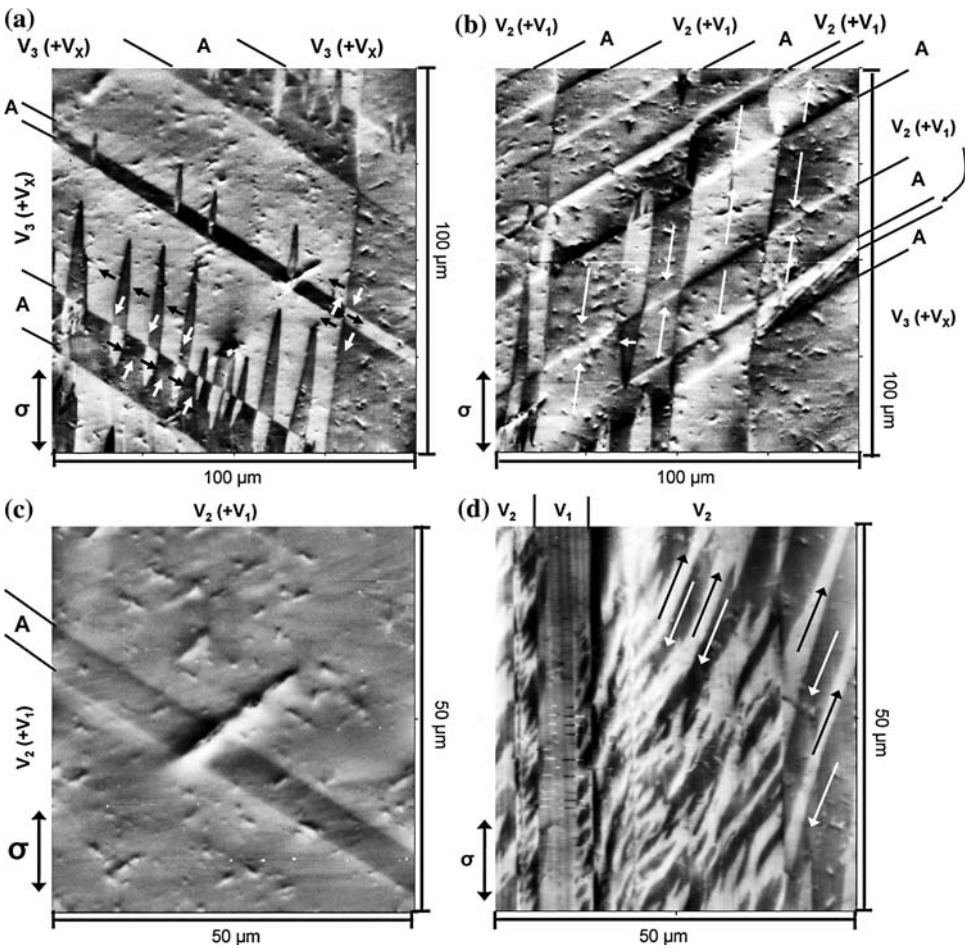

Fig. 8 MFM images of the thermo-mechanically trained crystal showing **a** a two-phase region of austenite (A) and martensite needles with higher volume fraction of twin variant V_3 recorded in the lower part in Fig. 4c at 1% strain, **b** austenite (A) and different martensite needles consisting of the twin variants V_1, V_2, V_3, and V_X at 1% strain corresponding to the upper left part of Fig. 4b, **c** a two-phase region of austenite (A) and fine internally twinned martensite matrix with higher volume fraction of martensite twin variant V_2 recorded in the left part in Fig. 5a at 3% strain, detwinned area with twin variants V_1 and V_2 at 3% strain corresponding to the lower left part of Fig. 5c. The arrows in **a**, **b**, and **d** represent the direction of magnetization

Discussion

Stress-induced martensite transformation and operant mechanisms

In SMAs the external loading leads to the formation of SIM from the parent austenite phase. Since the martensitic transformations lower the symmetry of a crystal without involving atomic exchange or diffusion, a single crystal of the parent phase is split into many twin-related domains called CVPs. As the SIM is associated with external stress, martensite variants with favorable orientation to the external loading direction will nucleate and grow obeying the resolved shear stress criterion [24, 36]. The selection of variants depends on several factors such as crystallographic orientation with respect to the loading direction, stress-state, temperature, chemical composition, and thermo-mechanical history of the material and the selected active variants govern the macroscopic.

The schematics in Fig. 9a and b summarize the microstructural evolution during the SIM transformation in the [001]-oriented Co–Ni–Ga crystals in their as-grown and trained state. While single internally twinned martensite is present in the as-grown state during the initial stages of the plateau region (1% strain), self-accommodating martensite is formed after training.

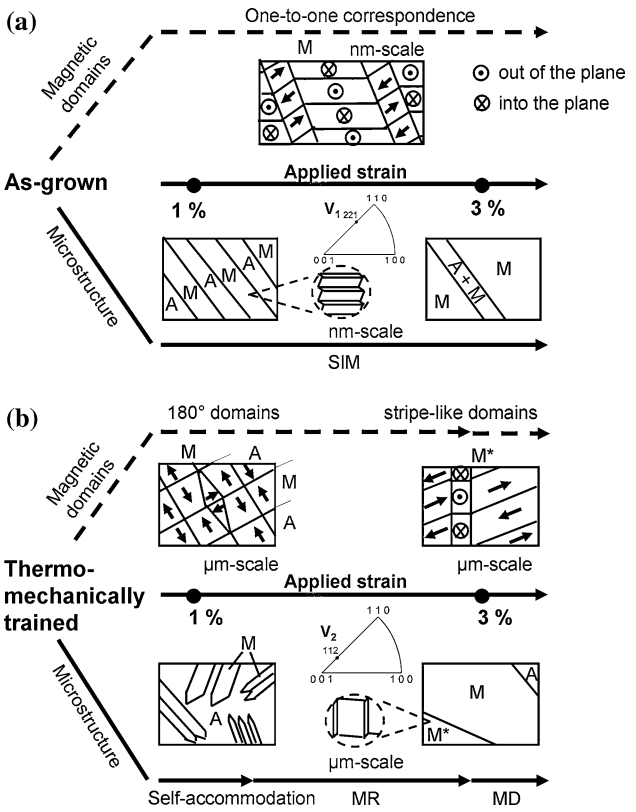

Fig. 9 Schematic illustrating the evolution of microstructure and magnetic domain morphology during stress-induced martensitic transformation in the [001]-oriented Co–Ni–Ga single crystals (**a**) before and (**b**) after the training. The inverse pole figures produced normal to the loading axis show the dominant variants. See main text for details

Macroscopically, the more uniform microstructure of the as-grown crystal (Fig. 9a) is reflected by the sharp transition from elastic deformation of austenite to the onset of SIM (Fig. 1a), whereas a continuous increase in stress up to the plateau regime is observed for the trained crystal (Fig. 1b). The reason for this change in macroscopic response is 2-fold. First, the interaction and competition among the various variants and martensite plates (Fig. 9b) should make the SIM transformation more difficult. However, the repeated phase transformation during training of the crystal is also accompanied by generation of defects such as dislocations. The motion of dislocations is curtailed in the<100>-oriented crystals due to the zero Schmid factor as the {110}<001>is the active slip system in B2 structured alloys [24]. The repeated pinning and depinning of propagating interfaces with these immobile dislocations during training will build up stress fields favorable for the nucleation of certain variants.

The initial self-accommodating microstructure present in the trained crystal first transforms into a single internally twinned martensite variant (V_2 in Fig 9b) trough a process called MR. MR occurs between different internally twinned martensite variants, giving way to the growth of most favorable ones at the expense of less ideally oriented ones [36]. Finally, martensite detwinning (MD) of the internally twinned martensite needles takes place (Fig. 9b). This mechanism will result in thickening of one of the variants of the CVP, i.e., the one with favorable orientation to the applied stress, via twin-boundary motion giving way to additional detwinning strains. MD is energetically less favorable as compared to MR, and thus, it only occurs at the later stages of the transformation [36, 37]. In the present study only partial detwinning has been observed and many regions of the sample still demonstrated twinned martensite at the higher strain of 3% (Fig. 5).

This is also expected based on theoretic calculations of the detwinning strains made elsewhere [24], which showed that detwinning is difficult in the case of compression along the [001] orientation.

Magneto-elastic coupling between magnetic domain configuration and microstructure evolution

The present results not only reveal that the martensite transformation mechanisms are different in the as-grown and in the thermo-mechanically trained crystal, but also show dissimilar magnetic domain configurations depending on the microstructural evolution, cf. Fig. 9. The structurally and magnetically homogenous state of the stress-free

austenite phase associated with low magnetic anisotropy energy resulting in a single large domain (Fig. 6a) is no longer present upon SIM transformation. In the as-grown crystal the magnetization direction varies from one twin to the other within a CVP and submicron magnetic domains with alternating magnetization directions are formed from the austenite's single magnetic domain state (Fig. 6b–d) as shown schematically in Fig. 9a. The resulting one-to-one correspondence between the magnetic domains and the twins observed in the SIM of as-grown Co–Ni–Ga alloys in this work (Fig. 7) is similar to results from Lorentz and OM studies that have been reported elsewhere [26, 27]. Nevertheless, the SIM of the present study showed more complicated domain patterns as compared to that of the thermo-elastic martensite studied by Chopra et al. [27].

Another interesting feature of the crystal in the as-grown state is the occurrence of magnetic domain structures in regions of residual austenite within the plateau regime (Fig. 6b and d). To find out whether these magnetic domain structures are stress-induced, an additional experiment was conducted within the elastic region of the austenite phase (Fig. 1a). The MFM-images demonstrated that the single magnetic domain state observed in the stress-free condition did not change by elastic deformation of the austenite. Thus, the existence of the magnetic domain structures in residual austenite within the PE-plateau regime is attributed to the formation of a precursor phase prior to the transformation to martensite. Similarly, Lorentz microscopy of magnetic domains in Heusler-type Co_2NiGa alloys revealed the presence of a precursor phase [25, 26]. De Graef et al. [25] have also observed that the magnetic modulation is on the same length scale as the structural tweed and attributed this correlation to magneto-elastic coupling between the magnetic domain structure and the microstructure before the onset of the martensitic transformation. By the same token, the observed micromagnetic domain reconfiguration from the single magnetic domain state of the austenite phase through a precursor phase highlights the presence of strong magneto-elastic coupling in present alloy. However, the structural changes between the austenite and the precursor phase are small and were not detectable with EBSD.

After the thermo-mechanical training, the trained crystal did not exhibit a one-to-one correspondence of the twin variants with the magnetic domains. Instead, the size of the magnetic domains became much larger, i.e., on the order of micrometers, and 180° domain walls coincide with the interfaces of martensite needles and residual austenite phases (cf. Figs. 8b and 9 b). The reason for this could be the difference in the morphology of the SIM of the as-grown crystal and the martensite present after thermo-mechanical training. Note that V_2 is the prominent twin-related variant after training. The one-to-one correspondence was reported to be dependent on the thickness of the twin plates [38]. The twin plates must reach a critical thickness to develop microdomains. This criterion has been verified by electron holography studies in a Fe–Pd alloy [15]. As the one-to-one correspondence was not observed in martensite present after training, it is concluded that the twin size is smaller than the critical thickness.

In addition fir tree patterns were observed at the low strain level of 1% (see Fig. 8a). These flux-collecting domain patterns arise when the surfaces are slightly mis-oriented with respect to the closest easy axis (less than about 5°) [38]. The domains then collect the net flux emerging from these mis-oriented surfaces. Similar observations are also reported for Ni–Mn–Ga alloys by Ge et al. [39] and were linked to the surface relief due to martensitic transformations.

Further transformation in the trained crystal to about 3% strain, has led to the growth of the twin variants V_1 and V_2 through MR, which in turn results in an almost structurally homogenous crystal. This gives rise to a single magnetic domain state similar to that of the austenite phase as seen in Fig. 8c. This can be achieved by migration and elimination of the 90° and 180° domain walls that were present initially at 1% strain (Fig. 9b). The coarsening of the twin variants due to detwinning as in Fig. 8d, give way to a stripe-like pattern with anti-parallel magnetization vectors as indicated by arrows, which also coincide with the interfaces of the twin variants V_1 and V_2. The magnetization vectors of the twin variant V_2 have perfect in-plane orientation in the right part of Fig. 8d. In the middle region of Fig. 8d the stripes proceed not in a straight-line manner due to very small local changes in the orientation of the twin variant V_2 parallel to the surface normal. The magnetic flux of the magnetic domains changes by about 90° at the twin boundaries and the magnetization vectors have out-of-plane orientation within the twin variant V_1. This kind of domain structure arises in microstructures consisting of alternating twins with high magnetic anisotropy energy [40].

Implications on the occurrence of magnetic field-induced strain (MFIS) in Co–Ni–Ga alloys under external stress

In the following, the occurrence of MFIS under constant external stress through phase and twin-boundary motion as well as martensite variant reorientation in the as-grown and thermo-mechanically trained Co–Ni–Ga-crystals will be discussed based on the different martensite formation mechanisms and the related magnetic domain configuration.

Magnetic field-induced strain through phase boundary motion could result from the growth of SIM in the as-grown crystal. The almost constant plateau stress indicates

that only a small change in stress is needed to increase the strain from 1% to 3% due to the growth of SIM (Fig. 1a). However, a low stress for phase boundary motion is not the only criterion for obtaining MFIS. The driving force for phase boundary motion due to external magnetic fields is the magnetic anisotropy of the martensite phase as compared to the austenite phase [7]. If the energy differences across the phase boundary are small, an applied magnetic field would only rotate the magnetization in both phases instead of propagating the phase boundary. In the as-grown condition both phases, austenite and martensite, show the micro-magnetic domain pattern. No distinct changes in magnetization are visible across the phase boundary between the martensite needles and residual austenite (Fig. 6b). Thus, it is unlikely that a phase boundary motion would occur in a magnetic field in these areas. However, at the interfaces between the martensite needles with higher volume fraction of variant V_2 and the residual austenite there is a clear variation in the overall magnetization direction (without considering the micro-domains) (Fig. 6d). A phase boundary motion by the application of a magnetic field appears feasible in these regions. Unfortunately, the martensite plates with higher volume fraction of the twin variant V_2 are scarce as V_1 is the dominant variant (Fig. 9a), thus, the aforementioned situation needed to observe MFIS may not occur in the present alloy in the as-grown state.

The thermo-mechanical training varies the magnetic domain configuration; still, no MFIS triggered by phase boundary motion will be obtained. The reason for this is the dominant 180° domain pattern (Fig. 9b), which coincides with the interfaces of the austenite and martensite phases. The 180° domain wall motion changes the magnetization but the shape of the crystal will be retained [7].

However, Co–Ni–Ga alloys provide an opportunity to demonstrate a stress-assisted magnetic field-induced twin-boundary motion. The as-grown crystal showed a one-to-one correspondence between the twin structure and the magnetic domains within the plateau regime. Thus, the magnetic domain structure is magneto-elastically coupled with the twin structure. When the variation in magnetic anisotropy energy between the twin variants (change in magnetization direction across the twin boundary) is sufficiently large, the application of a magnetic field could cause twin-boundary motion. However, detwinning is suppressed in compression along the [001] orientation [24]; thus, the stress for twin-boundary motion is very high and MFIS through twin-boundary motion within the plateau regime can hardly be obtained in the as-grown condition.

By contrast, MFIS by twin-boundary motion in the martensitic phase might result after thermo-mechanical training. Obviously, training decreased the stress for twin-boundary motion and at the high-strain level of about 3% partial detwinning finally occurred. Since the MR is mostly completed at this point, the additional transformation strain of about 1% is attributed to MD. The detwinned variants show a stripe-like domain pattern (Fig. 9b), which is a common feature in Ni–Mn–Ga alloys with high magnetic anisotropy energy. Therefore, the variation in magnetic anisotropy energy between the single magnetic domain state of the fine internally twinned martensite variants V_1 and V_2 and their detwinned variants should be high. The lower stress for twin-boundary motion in combination with the high anisotropy energy in the detwinned variants provide an opportunity for MSME. However, in the present crystals the volume fraction of the detwinned area is small resulting in only 1% strain. Future work will address this, and changes in temperature, an additionally thermo-mechanically training (increase of the numbers of cycles and/or stress levels) or a heat treatment are options to change the microstructure morphology of martensite variants to obtain a higher volume fraction for detwinning.

Conclusions

The results of the present study on the stress-induced martensitic transformation behavior and associated magnetic domain morphology of ferromagnetic Co–21Ni–30 Ga (at. %) single crystals can be summarized as follows:

1. The martensite formation under applied stress proceeds quite differently in the trained and untrained crystals. In the as-grown crystal SIM is formed and martensite variants with $[110]_M$ orientation parallel to the $[001]_A$ compression axis are favorable. After thermo-mechanical training MR is the main transformation mechanism, as a self-accommodated-like martensitic microstructure with multiple variants is formed right after the onset of the forward transformation. Subsequent to MR, partial detwinning occurs in the trained case at high-strain levels.
2. The different microstructural evolution has a pronounced effect on the magnetic domain configuration in both conditions. In the as-grown crystals the magnetic domains show a one-to-one correspondence with the martensite twin structure. In contrast, thermo-mechanical training leads to the formation of magnetic domains on the order of several micrometers, which do not show the same one-to-one correspondence. The domain walls coincide with the interfaces of martensite and residual austenite phases. The difference in magnetic domain morphologies is attributed to the variation in the thickness of martensite twins and the size of the twins after the thermo-mechanical training

is not sufficiently thick to show the one-to-one correspondence.

3. Provided that the volume fraction of detwinned martensite could be increased, a substantiated MFIS should originate from the detwinned areas, since the detwinned martensite variants show a stripe-like magnetic domain pattern with anti-parallel magnetization vectors, pointing to a high magnetic anisotropy.

Acknowledgements The present study was supported by Deutsche Forschungsgemeinschaft and US Army Research Office, Contract No W911NF-06-1-0319. The authors thank Prof. Y. I. Chumlyakov for providing the single crystals.

References

1. Ullakko K, Huang JK, Kanter C, O'Handley RC, Kokorin VV (1996) Appl Phys Lett 69:1966. doi:10.1063/1.117637
2. Heczko O, Sozinov A, Ullakko K (2000) IEEE Trans Magn 36:3266. doi:10.1109/20.908764
3. Sozinov A, Likhachev AA, Lanska N, Ullakko K (2002) Appl Phys Lett 80:1746. doi:10.1063/1.1458075
4. James RD, Wuttig M (1998) Philos Mag A 77:1273. doi:10.1080/01418619808214252
5. Fukuda T, Sakamoto T, Kakeshita T, Takeuchi T, Kishio K (2004) Mater Trans 45:188. doi:10.2320/matertrans.45.188
6. O'Handley RC (2000) Modern magnetic materials: principles and applications. Wiley-Interscience Publication, New York, p 260
7. O'Handley RC (1998) J Appl Phys 83:3263. doi:10.1063/1.367094
8. Likhachev AA, Sozinov A, Ullakko K (2004) Mater Sci Eng A 378:513. doi:10.1016/j.msea.2003.10.353
9. Heczko O (2005) J Magn Magn Mater 290–291:787. doi:10.1016/j.jmmm.2004.11.397
10. Pan Q, James RD (2000) J Appl Phys 87:4702. doi:10.1063/1.373134
11. Ge Y, Söderberg O, Hannula SP, Lindroos VK (2005) Smart Mater Struct 14:S211. doi:10.1088/0964-1726/14/5/007
12. Sullivan MR, Ateya D, Pirotta SJ, Shah AA, Wu GH, Chopra HD (2004) J Appl Phys 95:6951. doi:10.1063/1.1690197
13. Murakami Y, Shindo D, Oikawa K, Kainuma R, Ishida K (2002) Acta Mater 50:2173. doi:10.1016/S1359-6454(02)00061-7
14. Murakami Y, Shindo D, Oikawa K, Kainuma R, Ishida K (2004) Appl Phys Lett 85:6170. doi:10.1063/1.1841471
15. Murakami Y, Shindo D, Sakamoto T, Fukuda T, Kakeshita T (2006) Acta Mater 54:1233. doi:10.1016/j.actamat.2005.10.050
16. Karaman I, Karaca HE, Basaran B, Lagoudas DC, Chumlyakov YI, Maier HJ (2006) Scr Mater 55:403. doi:10.1016/j.scriptamat.2006.03.061
17. Karaca HE, Karaman I, Basaran B, Lagoudas DC, Chumlyakov YI, Maier HJ (2006) Scr Mater 55:803. doi:10.1016/j.scriptamat.2006.07.025
18. Karaca HE, Karaman I, Basaran B, Lagoudas DC, Chumlyakov YI, Maier HJ (2007) Acta Mater 55:4253. doi:10.1016/j.actamat.2007.03.025
19. Wuttig M, Li J, Craciunescu C (2001) Scr Mater 44:2393. doi:10.1016/S1359-6462(01)00939-3
20. Oikawa K, Ota T, Gejima F, Ohmori T, Kainuma R, Ishida K (2001) Mater Trans 42:2472. doi:10.2320/matertrans.42.2472
21. Chernenko VA, Pons J, Cesari E, Perekos AE (2004) Mater Sci Eng A 378:357. doi:10.1016/j.msea.2003.10.361
22. Dadda J, Maier HJ, Karaman I, Karaca HE, Chumlyakov YI (2006) Scr Mater 55:663. doi:10.1016/j.scriptamat.2006.07.005
23. Dadda J, Canadinc D, Maier HJ, Karaman I, Karaca HE, Chumlyakov YI (2007) Philos Mag 87:2313. doi:10.1080/14786430601175524
24. Dadda J, Maier HJ, Niklasch D, Karaman I, Karaca HE, Chumlyakov YI (2008) Metall Mater Trans A 39:2026. doi:10.1007/s11661-008-9543-0
25. De Graef M, Kishi Y, Zhu Y, Wuttig M (2003) J Phys IV 112:993. doi:10.1051/jp4:20031048
26. Saxena A, Castán T, Porta M, Kishi Y, Lograsso TA, Viehland D, Wuttig M, De Graef M (2004) Phys Rev Lett 92:197203-1-4
27. Chopra HD, Sullivan MR (2005) Rev Sci Instrum 76:013910-1-6
28. Sullivan MR, Pirotta SJ, Chernenko VA, Wu GH, Balasubramanium G, Hua SZ et al (2005) Int J Appl Electromagn Mech 22:11
29. Chikazumi S (1964) Physics of magnetism. Wiley, Inc., New York, p 117
30. Oikawa K, Ota T, Imano Y, Omori T, Kainuma R, Ishida K et al (2006) Equilib Diffus 27:75. doi:10.1361/105497106X92835
31. Cong DY, Zhang YD, Wang YD, Humbert M, Zhao X, Watanabe T et al (2007) Acta Mater 55:4731. doi:10.1016/j.actamat.2007.04.045
32. Sullivan MR, Chopra HD (2004) Phys Rev B 70:094427-1-8
33. Sullivan MR, Shah AA, Chopra HD (2004) Phys Rev B 70:094428-1-8
34. Liu CM, Chen LW (2005) J Phys D: Appl Phys 38:1182
35. Su F, Wei J, Liu Y (2005) Nanotechnology 16:1681. doi:10.1088/0957-4484/16/9/045
36. Gall K, Tyber J, Brice V, Frick CP, Maier HJ, Morgan N (2005) J Biomed Mater Res 75A:810. doi:10.1002/jbm.a.30464
37. Sehitoglu H, Hamilton R, Canadinc D, Zhang XY, Gall K, Karaman I et al (2003) Metall Mater Trans A 34:5. doi:10.1007/s11661-003-0203-0
38. Hubert A, Schäfer R (2000) Magnetic domains. Springer, Berlin, p 292, 422
39. Ge Y, Heczko O, Söderberg O, Hannula SP (2006) Scr Mater 54:2155. doi:10.1016/j.scriptamat.2006.02.037
40. Chernenko VA, Lvov VA, Besseghini S, Murakami Y (2006) Scr Mater 55:307. doi:10.1016/j.scriptamat.2006.04.038